

I. INTRODUCTION

The scanning electron microscope (SEM) is a type of microscope that produces images using signals generated from the interaction between electrons and the surface under observation. Higher resolution can be achieved compared to the traditional optical microscope, since electrons have much lower wavelength than light. An SEM can have resolution lower than one nanometre, whereas that of an optical microscope is often limited to a few hundred nanometres. This has benefited a variety of fields. For example, scientists have been using the SEM to analyse the doping density in semiconductors [1] and to view changes in bacterial cells [2].

Fig. 1 shows the basic construction of an SEM. The electron gun generates an electron beam, which is transformed into an electron probe after passing through the condenser lens and objective lens. It is scanned across the specimen under the effect of the scanning coil. As a result of the interaction between the incident electrons and the specimen, some electrons are emitted from the specimen. These are called secondary electrons and are collected by the detector, which generates signals whose magnitude depend on the strength of the secondary electrons. The display unit

produces one frame of image after each complete scan of the specimen.

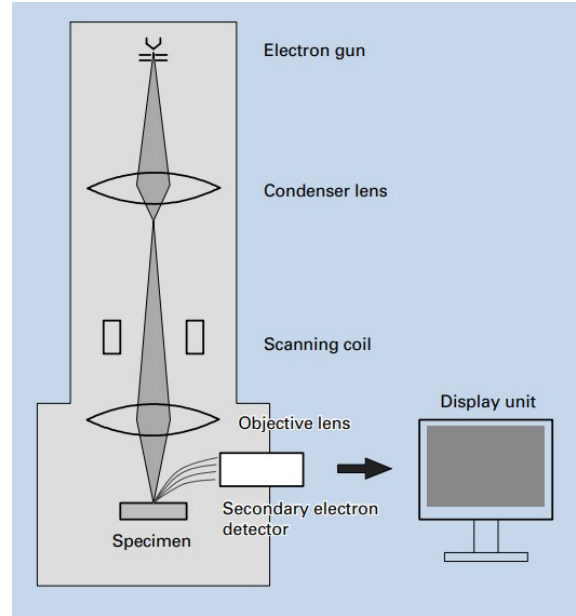


Fig. 1: Basic construction of an SEM [3].

Digital image analysis methods have been widely used in the field of SEM. For example, the fibre orientation distribution of non-woven fabrics can be determined using fast Fourier transform (FFT) and Hough transform (HT) [4]. The FFT is an especially popular algorithm and many papers have been published on the use of it. However, due to its complexity and a lack of fast hardware, real-time analysis had largely been impossible or impractical in the past, i.e. it was only feasible to perform FFT on images off-line. In 1997, with an advanced central processing unit (CPU) — the Pentium Pro, it was only possible to achieve a refresh rate of about 0.6

frames per second for an 8-bit 1024×1024 image [5]. The enhancement of CPUs has enabled faster frame rates and more recently, the development of graphics processing unit (GPU) has taken image analysis to a different level.

The GPU was originally designed to efficiently manipulate data in order to accelerate the rendering of 3D images on displays. Depending on the position, pixels in a 3D image may require different processing to achieve effects such as lighting, blurring and fogging. This is achieved by breaking down the image into a massive number of fragments and processing each fragment individually. The processes happen independently but may share the same logical sequence of control, and this pattern is named single instruction multiple data (SIMD). A GPU consists of a large array of processing cores, with each of them using SIMD to process a block of fragments.

The characteristic of the GPU allows it to outperform central processing units (CPUs) when performing algorithms that manipulate data in parallel. Take the dot product between two vectors of size 1000 as an example, the processing cores on the GPU may be 100 times slower than the CPU, but if 1000 of them work in parallel and each computes the multiplication of one element from each vector, the overall speed will be 10 times

faster. This has allowed computer vision programs that were previously impossible or computationally too expensive to build. For example, a wearable mediated reality device that make computer-generated information appear to the user as though it was anchored in the real world [6].

The goal of the project is to develop software tools based on fast computation provided by the GPU, to support interactive real-time diagnosis of SEM images for the purpose of assisting the operator or automating procedures, with a focus on the use of FFT.

II. SOFTWARE ASPECTS OF THE TOOLS

A. *Design principle*

Considering that the work of the project may serve as the foundation stone for many further developments, the design of the software has a strong emphasis on readability and maintainability.

B. *The selection of programming language*

The SEM used for the project is made by Carl Zeiss AG, which provides an application programming interface (API) that can be used for controlling the SEM and grabbing images from it. The API supports C++ and thus makes it a possible programming language for the project. Being a relatively low-level compiled language makes

C++ extremely fast and useful for speed-critical applications. However, it also means that C++ has a complex syntax, which could significantly slow down development if the user does not have enough experience with it.

Considering the time scale of the project and to make development easier for people who will continue the work, Python is selected instead as the programming language, which has a much simpler syntax and is widely supported. With careful design, it has proved to be able to produce useful results despite the slower speed (see later sections).

C. Modules of the software

The software is highly modularised, which maximises readability and maintainability. This also makes it easier to translate the programs into C++ later if better performance is needed, since C++ is mostly used in an object-oriented manner. Fig. 2 shows the six main classes of the software.

SEM_API is a Python wrapper for the native SEM API written by Luyang Han, which allows the user to directly control the SEM in Python.

SemImage encapsulates variables and methods that are directly relevant to an image taken by the SEM, and *SemImageGrabber* is a helper class that helps obtain image data from the SEM and

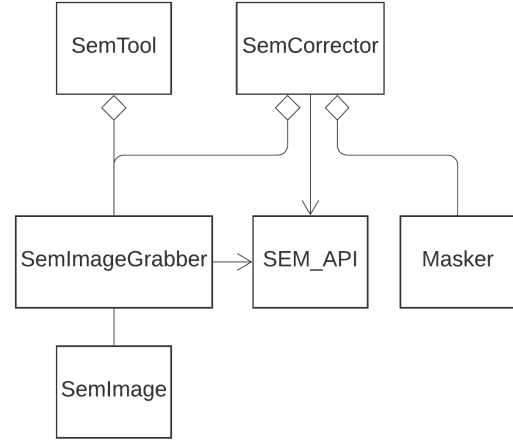


Fig. 2: Class diagram of the software in unified modelling language (UML).

create instances of *SemImage* from them.

Images can be obtained in two ways:

- From the SEM.
- From a local folder, which is helpful when the SEM is not available.

SemImageGrabber detects if the SEM is available and decides on which way to use.

SemTool handles the creation and rendering of the graphical user interface (GUI). Fig. 3 shows a screenshot of the control panel. The push buttons open a window for the corresponding plot and the radio buttons select algorithms (see section III and IV for detailed descriptions) to be performed on the image. The plots are shown on different windows, and can be opened and closed individually. This improves framerate by allowing the user to close unneeded windows, and also makes

it easier to add other plots later. Table I shows that the improvement is rather significant, as rendering windows is a major time-consuming process of the software. When only one window is opened, a refresh rate of about 16 frames per second is possible.

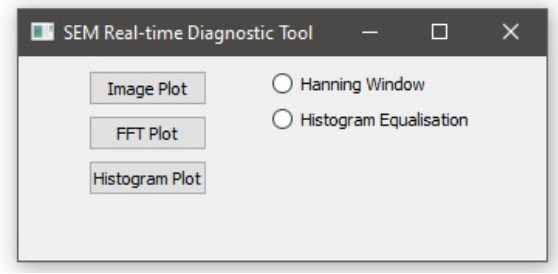


Fig. 3: Screenshot of the GUI.

TABLE I: Results of software framerate test

Number of windows opened	Time taken to update each frame
zero	15 ms
one	60 ms
three	160 ms

^aThe numbers are approximate.

^bWith 8-bit grey-scale 1024 × 768 input images.

^cWith Intel Core i7 and NVIDIA GeForce GTX 1060.

SemCorrector implements the automatic focusing and astigmatism correction algorithm and uses a helper class *Masker* to achieve fast computation (see section V for detailed descriptions). Due to the impact of the COVID-19 pandemic, the algorithm has not been fully tested, and is therefore not integrated to the GUI yet.

III. REAL-TIME HISTOGRAM EQUALISATION FOR IMPROVING IMAGE CONTRAST

There are many types of histograms in image processing. The grey level (brightness level) pixel intensity histogram, which plots the number of pixels of each grey value in the image, is the most relevant one for SEM images. This is because an SEM translates the energy of the secondary electrons directly into a grey level, colours do not exist in SEM images.

The algorithm for obtaining the histogram of an SEM image is given by

$$n_l = \frac{1}{P} \sum_p I(l_p = l), \quad (1)$$

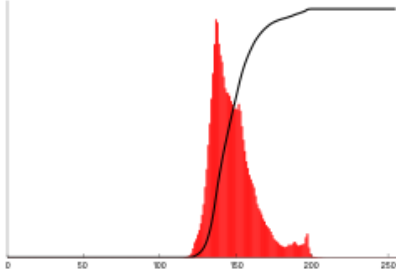
where n_l is the normalised number of pixels of grey level l , P is the total number of pixels in the image and l_p is the grey level of the p_{th} pixel.

Fig. 4a shows an 8-bit grey-scale image, i.e. its depth of digitisation is 8-bit and it has 256 grey levels. Fig. 4b shows the histogram of the image and its integral. As can be seen in the histogram, most pixels are concentrated in the middle of the grey scale. This is reflected by the fact that the image is missing its highlights and shadows.

Histogram equalisation is a method for adjusting the distribution of pixel intensities of an image, in order to improve its overall



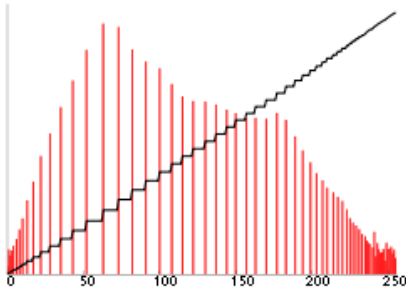
(a) Original image.



(b) Histogram of the original image.



(c) Histogram-equalised image.



(d) Histogram of the histogram-equalised image.

Fig. 4: Histogram and histogram equalisation.

contrast. Effectively, it is achieved by spreading out the more frequent intensity values. To perform histogram equalisation, first obtain the integral of the histogram using

$$s_l = \sum_{i=1}^l n_i,$$

where s_l is the value of the integral at grey level l . The integral spans from 0 to 1 as the histogram is normalised. Scale the integral by the maximum grey level and perform rounding to create the transform function

$$f_l = \lfloor s_l L \rfloor, \quad (2)$$

If a pixel in the original image has grey level l , it will have grey level f_l in the transformed image. For example, if all pixels in the original image are concentrated between grey level 100 to 200, the pixels of level 100 will become 0 in the new image while the pixels of level 200 will become 255 (assuming 8-bit image).

The result is more noticeable when the image has a low contrast, such as the one shown in Fig. 4a. The histogram-equalised version of it is given in Fig. 4c and the new histogram in Fig. 4d. More details are now visible as the contrast has been enhanced.

The most time-consuming part of histogram equalisation is to map all pixels in the original image to their new values using the transform function (2). This can be implemented using CPU code in one line:

`newImage =`

```
map(lambda x: f[x], image)
```

f is an array that serves as the transformation function, if the original pixel value is x , the new value should be $f[x]$. The `lambda` operator is a way to create small anonymous functions, which are throw-away functions and are only needed where they are created. It improves conciseness and readability by reducing code bloat. `lambda x: f[x]` creates an anonymous function that returns $f[x]$ when given x , and `map()` uses this function to transform all pixels in `image`. This gives a time complexity of $O(N^2)$ which is not optimal. A smaller time complexity can be achieved using the GPU code:

```
map = cupy.ElementwiseKernel(
    'T x, raw T f', 'T xNew',
    'xNew = f[x]',
    'map'
)
newImage = map(image, f)
```

`cupy.ElementwiseKernel()` defines a kernel that the GPU uses to process the input data in parallel. Tests have shown that the use of GPU can increase the speed by 2 times, as summarised in Table II. In theory, the factor of speed improvement should be similar as that for calculating the histogram, since it also requires iterating through all pixels in the image. However, the code implementations introduce overheads which limit

the improvement in speed.

TABLE II: Speed comparison between CPU and GPU

Algorithm	Time taken using CPU	Time taken using GPU
Apply Hanning window	16 ms	9 ms
Calculating histogram	30 ms	2 ms
Histogram equalisation	9 ms	5 ms
Fast Fourier transform	60 ms	8 ms

^bFor an 8-bit grey-scale 1024×768 input image.

^cWith Intel Core i7 and NVIDIA GeForce GTX 1060.

IV. REAL-TIME FAST FOURIER TRANSFORM FOR EVALUATING IMAGE FOCUSING AND ASTIGMATISM

The quality of an SEM image is affected by aberrations. While some exist because of the fundamental properties of the microscope and are difficult to get rid of, some can be completely eliminated by adjusting relevant settings. Two important ones are focus and stigmator control, which directly affect the resolution and astigmatism of the image, respectively. Fig. 5 illustrates the effect of wrong focus and stigmator settings.

Focus determines the focal point of the electron probe. When the focal point is far from the surface of the specimen, the incident electrons interact with the specimen in a larger area. As a result, spots near each other

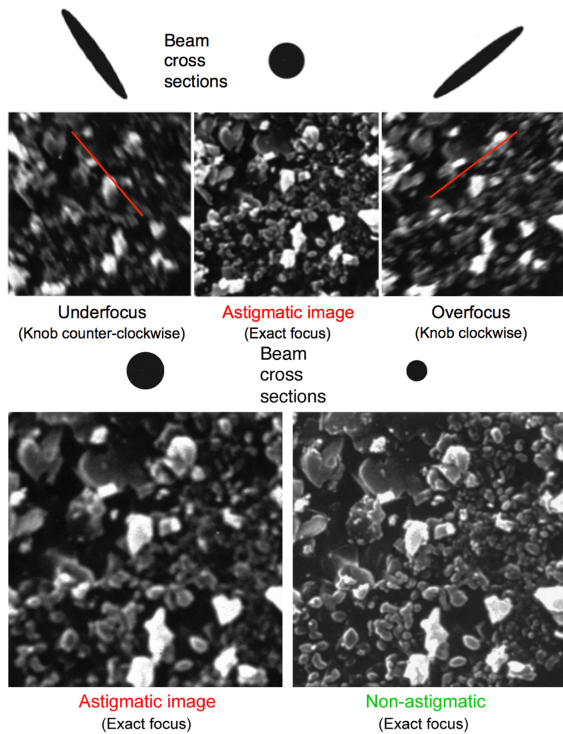


Fig. 5: Sample astigmatic SEM images [7].

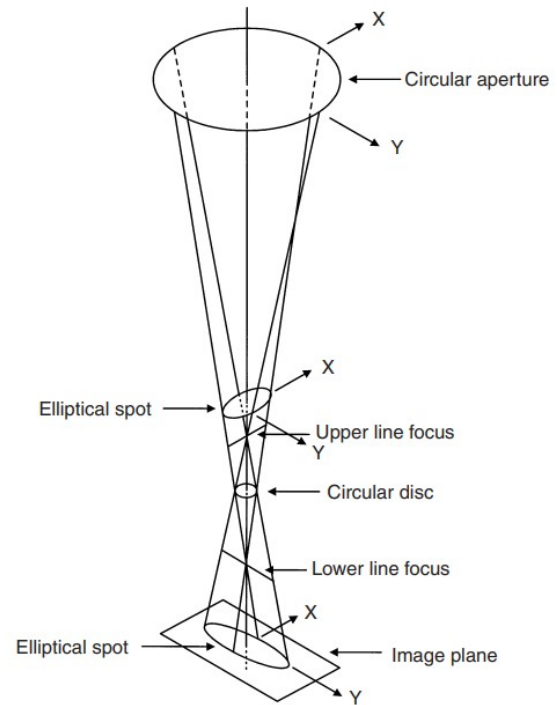


Fig. 6: Uneven focus of the SEM.

produce signals of closer magnitude. This makes the image appear blurry.

Stigmators are used to compensate for astigmatism. Astigmatism arises due to imperfections in components of the SEM, and describes uneven focus in the electron probe, as shown in Fig. 6. When the electron probe is out of focus, astigmatism makes the incident electrons interact with the specimen in an elliptical area, and thus makes the image appear stretched. When the electron probe is in focus, astigmatism makes the image appear blurry.

Although experienced SEM operators can often find the right settings for focus and

stigmator control in a short time, it may not be as straightforward for new users. The complexity arises because any judgement of an image is based on what the operators see through their eyes, which is rather subjective. Sometimes, the surface being observed may have a complex structure and makes adjusting even harder. Intensive training and practical experience are often required for an operator to become efficient in using the SEM.

The Fourier transform (FT) decomposes a function into its constituent frequencies, as illustrated in Fig. 7. The function in red is can be represented by a superposition of all

the sinusoidal functions shown, each having a unique frequency and with magnitudes as indicated on the right panel. A function that changes more abruptly will have stronger high-frequency components than a smoother one.

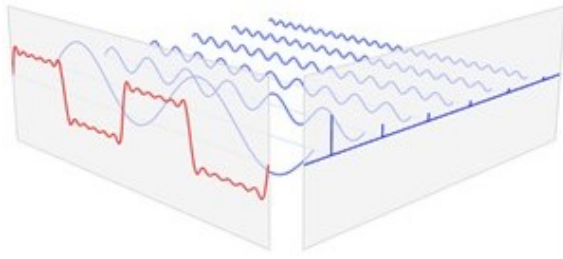


Fig. 7: Fourier transform.

In image processing, the discrete Fourier transform (DFT) is often preferred, which takes a finite sequence of equally-spaced values as input and is thus better suited than the FT. It is defined by

$$X_k = \sum_{n=0}^{N-1} x_n \cdot e^{-i2\pi kn/N}, \quad 0 \leq k \leq N-1, \quad (3)$$

where x_0, x_1, \dots, x_{N-1} is the input sequence and X_0, X_1, \dots, X_{N-1} is the output sequence. X_k is effectively the result of the dot product between the vector $[x_0, x_1, \dots, x_{N-1}]$ and $[e^0, e^{-i2\pi k/N}, \dots, e^{-i2\pi k(N-1)/N}]$, and the latter is a finite sequence of frequency $2\pi k$. Therefore, the DFT computes the magnitude of

the component of the input sequence with frequency $2\pi k$, for $0 \leq k \leq N-1$.

Fig. 8 gives an example of FFT applied on a real image. The top row shows a set of images and the bottom row shows the corresponding transforms (amplitudes only). Points near the origin represent lower-frequency components and are cut off when a high-pass filter is applied to the image.

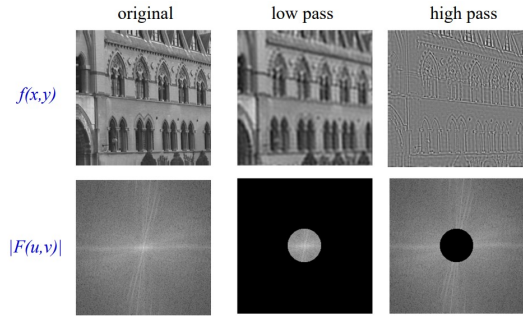


Fig. 8: FFT and filtering on images [8].

A drawback of using (3) is that it has a time complexity of $O(N^2)$. In image processing, where the inputs are 2D sequences, the time complexity quickly explodes and makes the equation practically impossible to use. A fast Fourier transform (FFT) is an algorithm that computes the DFT with smaller timer complexity. There are many feasible algorithms and all known ones have complexity $O(N \log N)$. Detailed discussion on FFT algorithms is beyond the scope of this report.

The focusing and astigmatism of an SEM image can be evaluated using its FFT. Fig.

10 provides a set of sample images that illustrate how different degrees of defocus and astigmatism affect the image and its FFT. An in-focus image contains more details, and its FFT will thus have stronger high-frequency components. As an astigmatic image goes from under-focus to over-focus, the elliptical incidence area of the electron probe rotates by 90 degrees and makes the image appear stretched in the new direction. As a result, its FFT also rotates by 90 degrees.

An image is effectively a finite sequence of data, and this can cause boundary effect when its FFT is calculated. The abrupt discontinuity at the edges gives the FFT some strong high-frequency components. To circumvent this, the *SemImage* class provides two methods — `applyHamming()` and `applyHanning()`, which apply a Hamming and Hanning window function to the image data, respectively. The window functions taper the edges off towards zero, and thus reduce the boundary effect. Fig. 9 illustrates how they look like, and they can be obtained by setting a_0 to 0.5 and 25/46, respectively, in the function

$$w[n] = a_0 - (1 - a_0) \cdot \cos \frac{2\pi n}{N}, \quad 0 \leq n \leq N. \quad (4)$$

As summarised in table II, the use of GPU can make the calculation of FFT eight times faster. Without the GPU, calculating FFT

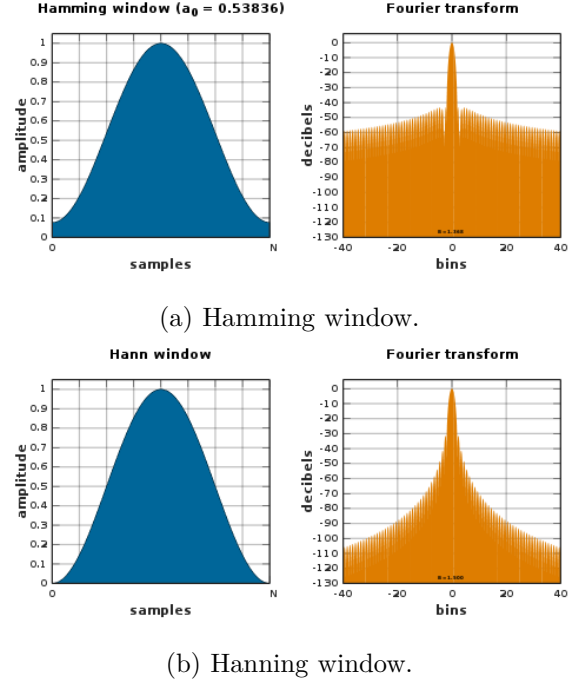


Fig. 9: Window functions.

alone limits the refresh rate of the tool to 16 frames per second. The GPU changes the number to 125 frames per second.

V. AUTOMATIC FOCUSING AND ASTIGMATISM CORRECTION ALGORITHM

K.H. Ong, J.C.H. Phang and J.T.L. Thong proposed an algorithm for automatic focusing and astigmatism correction [9] using the properties of the FFT of SEM images described in section IV.

The FFT of an image can be converted into a binary image by applying a threshold to the magnitudes, and segmented into 8 regions as shown in Fig. 11. A pixel has value 1 if the magnitude is above the threshold and

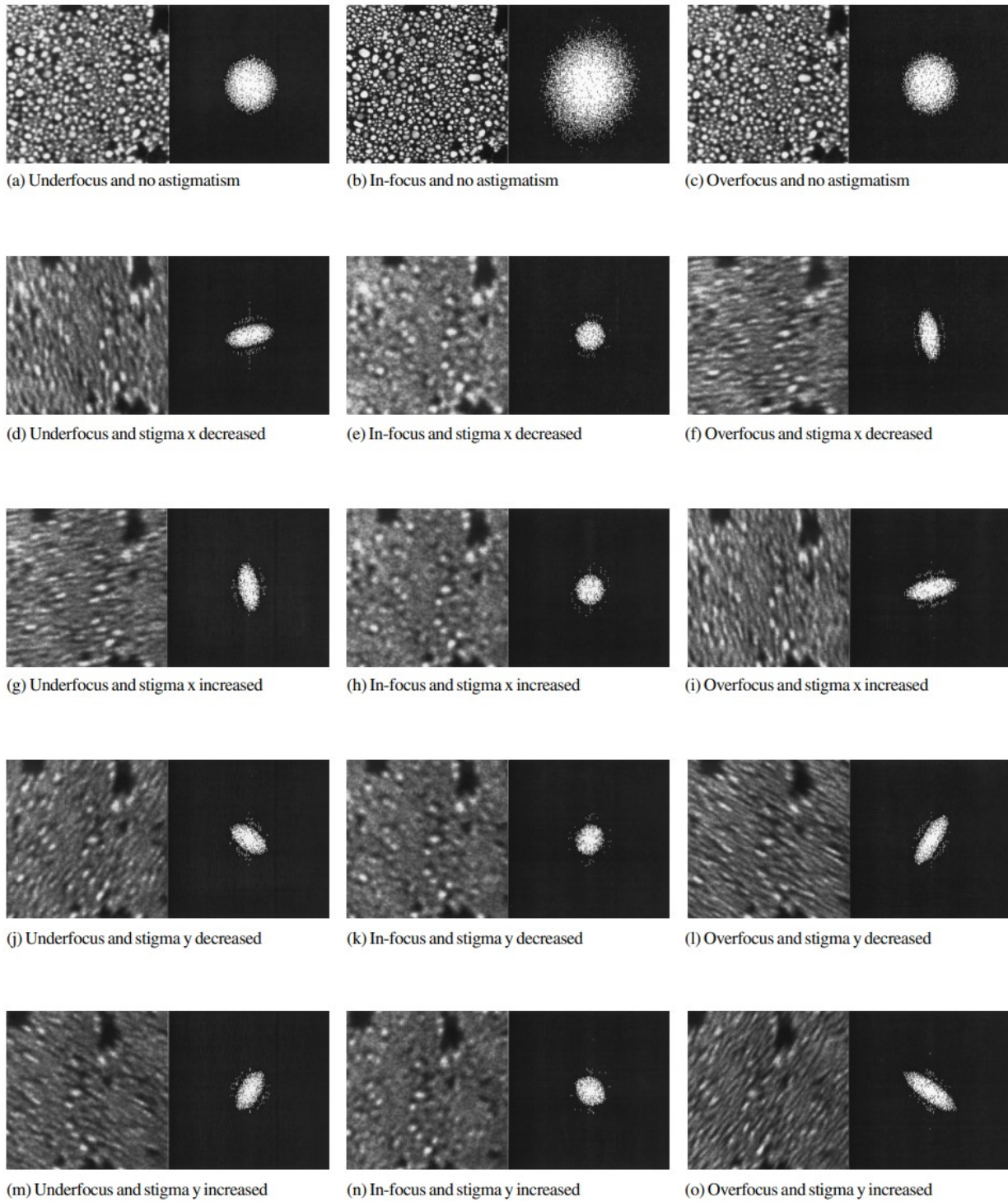


Fig. 10: Images of gold-on-carbon sample and their fast Fourier transforms (FFTs) for different degrees of defocus and astigmatism [9].

0 otherwise. Let I be a matrix representing the current image with focal length set to F , obtain an under-focused image I_{uf} and over-focused image I_{of} by setting the focal length to $F - \Delta F = F_{uf}$ and $F + \Delta F = F_{of}$, respectively. Let T , T_{uf} and T_{of} be matrices representing the binary FFT of I , I_{uf} and I_{of} , respectively.

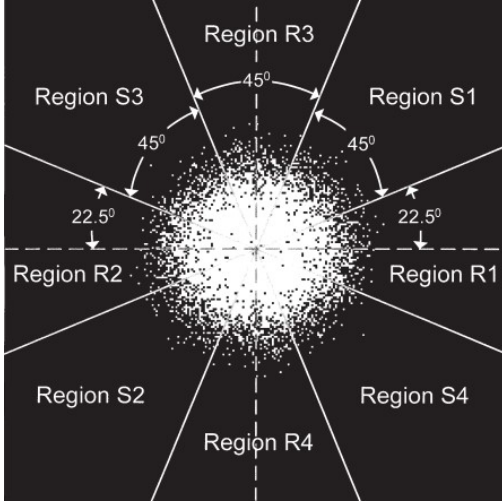


Fig. 11: Segmented fast Fourier transform [9].

The focal length can be adjusted by comparing the sum of pixel values in T , T_{uf} and T_{of} . Let the perfect focal length for the image be \hat{F} , then

$$\begin{cases} \text{sum}(T_{of}) < \text{sum}(T) < \text{sum}(T_{uf}), & \hat{F} < F_{uf} \\ \text{sum}(T_{of}) < \text{sum}(T_{uf}), & F_{uf} < \hat{F} < F \\ \text{sum}(T_{of}) = \text{sum}(T_{uf}) < \text{sum}(T), & F = \hat{F} \\ \text{sum}(T_{uf}) < \text{sum}(T_{of}), & F_{of} > \hat{F} > F \\ \text{sum}(T_{uf}) < \text{sum}(T) < \text{sum}(T_{of}), & \hat{F} > F_{of} \end{cases}.$$

Let

$$P = \text{sum}(T_{of}) - \text{sum}(T_{uf}). \quad (5)$$

Then, the rules for adjusting focal length are

- when $P > 0$, the focal length should be decreased.
- when $P < 0$, the focal length should be increased.

After the focal length has been set to the perfect value, i.e. when $F = \hat{F}$, the stigmator settings can be determined by comparing the sum of pixel values in different regions of T , T_{uf} and T_{of} . The rules for adjustment can be determined using Fig. 10. Let

$$P_{R12} = \text{sum}(FI_{of,R12}) - \text{sum}(FI_{uf,R12}), \quad (6)$$

$$P_{R34} = \text{sum}(FI_{of,R34}) - \text{sum}(FI_{uf,R34}), \quad (7)$$

$$P_{S12} = \text{sum}(FI_{of,S12}) - \text{sum}(FI_{uf,S12}), \quad (8)$$

$$P_{S34} = \text{sum}(FI_{of,S34}) - \text{sum}(FI_{uf,S34}). \quad (9)$$

Then the rules for adjusting stigmator settings are

- when $P_{R12} > 0$ and $P_{R34} < 0$, the value of stigmator x should be decreased.
- when $P_{R12} < 0$ and $P_{R34} > 0$, the value of stigmator x should be increased.
- when $P_{S12} > 0$ and $P_{S34} < 0$, the value of stigmator y should be increased.
- when $P_{S12} < 0$ and $P_{S34} > 0$, the value of stigmator y should be decreased.

Fig. 12 shows the general flow chart of the algorithm.

A key factor that affects the performance of the automatic focusing and astigmatism correction algorithm is the speed of perform-

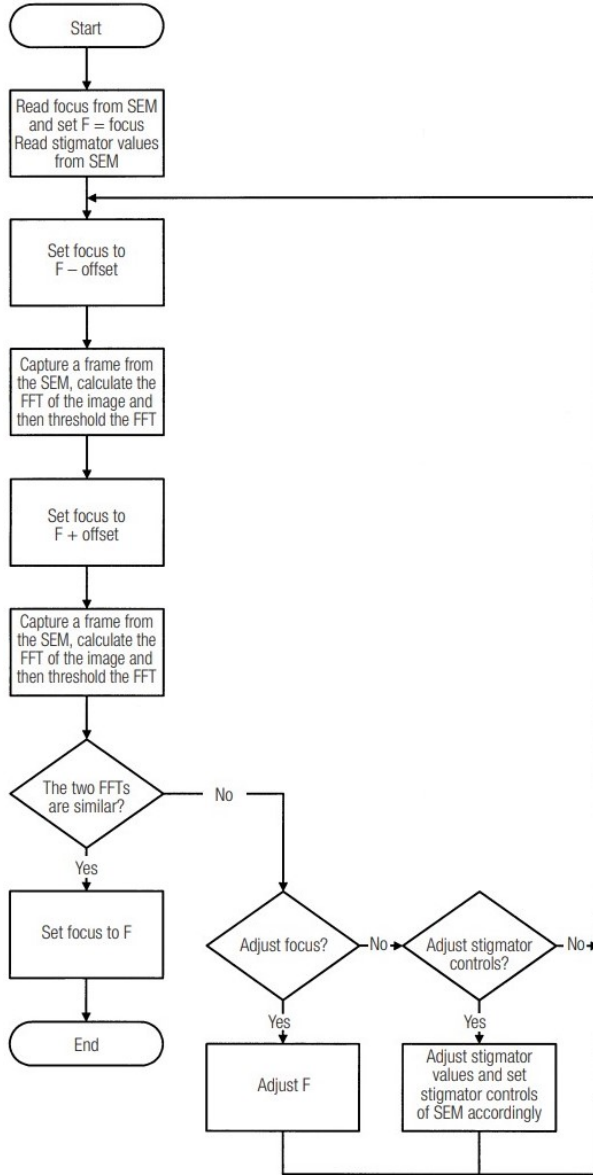


Fig. 12: General flow chart of the correction algorithm [9].

ing segmentation on the FFTs. The most straightforward way of doing it is to iterate through the whole matrix while calculating the sums in pure Python, for every FFT. This has a time complexity of $O(N^2)$. The *Masker* module provides a faster solution.

A *Masker* can be initialised with a 2D shape, and it will create eight matrices, each representing a region as shown in Fig. 11. For example, if the input is [5, 7], the matrix created for region R1 will be

$$\begin{bmatrix} 1 & 1 & 1 & 1 & 1 & 1 & 1 \\ 1 & 1 & 1 & 1 & 1 & 1 & 0 \\ 1 & 1 & 1 & 0 & 0 & 0 & 0 \\ 1 & 1 & 1 & 1 & 1 & 1 & 0 \\ 1 & 1 & 1 & 1 & 1 & 1 & 1 \end{bmatrix}.$$

The algorithm ensures that there is no overlapping between matrices apart from at the center. After obtaining the matrix for region R1, the sum of values in an FFT in R1 can be calculated using:

```
ma.array(fft, masker.r1).sum()
```

VI. CONCLUSIONS

REFERENCES

- [1] T. Agemura and T. Sekiguchi, "Secondary electron spectroscopy for imaging semiconductor materials," 2018 International Symposium on Semiconductor Manufacturing (ISSM), Tokyo, Japan, 2018, pp. 1-3, doi: 10.1109/ISSM.2018.8651171.
- [2] T. Cushnie, N. O'Driscoll and A. Lamb, "Morphological and ultrastructural changes in bacterial cells as an indicator of antibacterial mechanism of action," Cellular and Molecular Life Sciences, 2016, vol. 73, no. 23, pp. 4471-4492, doi: 10.1007/s00018-016-2302-2.
- [3] "SEM A to Z," Jeol.co.jp, [Online], available: https://www.jeol.co.jp/en/applications/pdf/sm/sem_atoz_all.pdf. [Accessed: 18 May 2020].

- [4] E. Ghassemieh, M. Acar and H. Versteeg, "Microstructural analysis of non-woven fabrics using scanning electron microscopy and image processing. Part 1: Development and verification of the methods," *Proceedings of the Institution of Mechanical Engineers, Part L: Journal of Materials: Design and Applications*, 2002, vol. 216, no. 3, pp. 199-207, doi: 10.1177/146442070221600305.
- [5] A. Vladár, M. Postek and M. Davidson, "Image sharpness measurement in scanning electron microscopy-part II," *Scanning*, 2006, vol. 20, no. 1, pp. 24-34, doi: 10.1002/sca.1998.4950200104.
- [6] J. Fung, F. Tang and S. Mann, "Mediated reality using computer graphics hardware for computer vision," *Proceedings. Sixth International Symposium on Wearable Computers*, Seattle, WA, USA, 2002, pp. 83-89, doi: 10.1109/ISWC.2002.1167222.
- [7] C. Lyman, "Correcting Astigmatism in SEM Images," *Microscopy Today*, 2019, vol. 27, no. 03, pp. 32-35, doi: 10.1017/s1551929519000476.
- [8] "2D Fourier transforms and applications," *University of Oxford*, 2014, [Online], available: <http://www.robots.ox.ac.uk/>. [Accessed: 19 May 2020].
- [9] K.H. Ong, J.C.H. Phang and J.T.L. Thong, "A robust focusing and astigmatism correction method for the scanning electron microscope," 1997, *scanning* 19: 553-563, doi: 10.1002/sca.4950190805.